Journal of
Materials Chemistry A

Accepted Manuscript

This article can be cited before page numbers have been issued, to do this please use: M. Stringer, J. E. Bishop, J. A. Smith, D. K. Mohamad, A. Parnell, V. Kumar, C. Rodenburg and D. G. Lidzey, *J. Mater. Chem. A*, 2017, DOI: 10.1039/C7TA03103C.

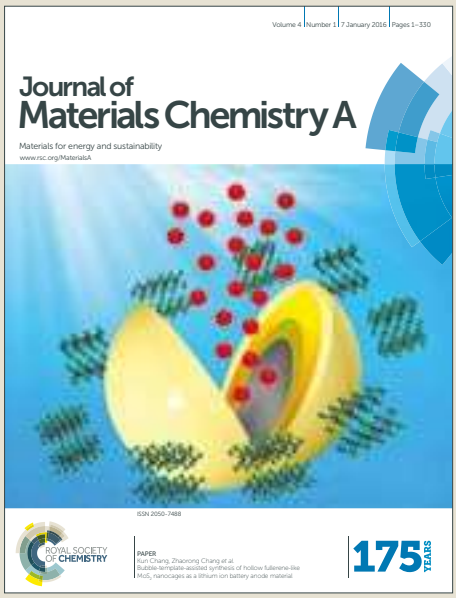

ROYAL SOCIETY OF CHEMISTRY

rsc.li/materials-a

View Article Online
DOI: 10.1039/C7TA03103C

DOI: 10.1002/ ((please add manuscript number))

Article type: (Full Paper)

Efficient perovskite photovoltaic devices using chemically doped PCDTBT as a hole-transport material

Michael Wong-Stringer[1], James E. Bishop[1], Joel A.Smith[1], David K. Mohamad[1], Andrew J. Parnell[1], Vikas Kumar[2], Conny Rodenburg[2] and David G. Lidzey[1]*

1) Department of Physics & Astronomy, University of Sheffield, Hicks Building, Hounsfield Road, Sheffield, S3 7RH, U.K.

2) Department of Chemical and Biological Engineering, University of Sheffield, Mappin St, Sheffield, S1 3JD

*Corresponding author, email d.g.lidzey@sheffield.ac.uk

Keywords: PCDTBT, perovskite solar cells, p-doping, conductivity, hole-transport materials

Abstract

It is shown that by chemically doping the carbazole-based conjugated polymer PCDTBT using the molecular materials TBP, LiTFSI and FK209, its conductivity can be increased by a factor of 10^5 times. Such doped PCDTBT films are used as a hole transport material (HTM) for standard architecture $(CH(NH_2)_2PbI_3)_{0.85}(CH_3NH_3PbBr_3)_{0.15}$ perovskite solar cells (PSCs). We show that devices with optimised PCDTBT thickness and doping level achieve a peak power conversion efficiency (PCE) of 15.9%. We expect a number of related doped conjugated polymers to also be capable of acting as efficient HTMs for PSCs.

View Article Online
DOI: 10.1039/C7TA03103C

1. Introduction

Over the last few years, perovskite solar cells (PSCs) have shown promising progress in terms of efficiency and stability. Stabilised power conversion efficiencies (PCEs) reaching 21.6% have been reported,[1] with devices operating for > 10,000 hours with no loss in performance demonstrated.[2] The choice of hole-transport materials (HTMs) used in perovskite devices is receiving increasing scrutiny, with research focused on maximizing charge-transport efficiency and operational stability, but minimising the cost and complexity of the HTM layer.[3,4]

In standard structure perovskite devices incorporating a device architecture of [glass/fluorine-doped tin oxide (FTO)/electron transport material (ETM)/perovskite/HTM/metal contact], the most commonplace HTM remains 2,2',7,7'-tetrakis[N,N-di(4-methoxyphenyl)amino]-9,9'-spirobifluorene (spiro-OMeTAD). However, to act as an efficient HTM, spiro-OMeTAD usually requires chemical doping. This involves adding a combination of several key chemicals, namely; 4-*tert*-Butylpyridine (TBP), bis(trifluoromethane)sulfonimide lithium salt (LiTFSI), and FK 209 Co(III) - TFSI salt (FK209), with the amounts added varying between publications.[5–7] A complete understanding on how exactly this cocktail of dopants affects the HTM and the rest of the device stack is not yet available. It is widely agreed that LiTFSI and FK209 dopants create a p-doped state on spiro-OMeTAD.[8–12] Here, the LiTFSI doping requires optical-radiation and oxygen to p-dope the spiro-OMeTAD; a process that increases its conductivity by over three orders of magnitude.[9,10] However recent work on the use of FK209 to dope other HTMs demonstrates that it can generate similar p-doped states in an inert atmosphere, without relying on light and oxygen.[1,6,9] It has been proposed that the additive TBP migrates through the perovskite stack and becomes located at the interface between the perovskite and the TiO_2; this passivates trap states at the TiO_2 surface, resulting in a negative shift in the TiO_2 conduction band states

View Article Online
DOI: 10.1039/C7TA03103C

which increases the device open circuit voltage (V_{oc}).[13] However, other work suggests that the LiTFSI passivates the TiO_2 surface, whilst TBP provides an increase in J_{sc} (and hence charge-collection efficiency) regardless of the choice of ETM or HTM.[14,15] Indeed, using the additive TBP in an HTM is thought to lead to an increase in hole selectivity via band bending at the perovskite/HTM interface; a process that is evidenced by a significant improvement (5.5% to 12%) in the stabilised power output of TBP-doped PSC devices.[15] It has also been demonstrated that TBP helps solubilize other dopants added to the HTM, thereby improving the wetting of the HTM onto the perovskite surface.[14] Gaining a deeper understanding of how these dopants and additives affect an entire device stack is thus an important part of the development of an efficient and stable PSC.

There have recently been reports that certain tailored "dopant-free" HTMs can almost match the efficiencies of spiro-OMeTAD,[11,16] however, the use of dopants generally appears to be an effective strategy to improve the charge-transport properties of many HTM materials.[3,4,17] Here, we explore the use of a chemically-doped film of the donor-acceptor carbazole co-polymer poly[N-9'-heptadecanyl-2,7-carbazole-alt-5,5-(4',7'-di-2-thienyl-2',1',3'-benzothiadiazole)] (PCDTBT) as a HTM in a perovskite solar cell. Organic heterojunction solar cells that use the popular material PCDTBT generally have excellent operational stability, with devices demonstrated to have Ts80 lifetimes of up to 6,200 hours when operating in outdoor conditions.[18] This stability results from its low-lying highest-occupied molecular orbital (HOMO) level, which is positioned at 5.45 eV[3,18–22]. We note that the HOMO-level of PCDTBT is in fact lower than that of the spiro-OMeTAD HOMO level (which has been reported in the range of 5.0 to 5.22 eV[3,23]), suggesting that it may have improved oxidative stability when incorporated as the HTM in PSC devices. Importantly, recent development of simpler routes to synthesize PCDTBT now allow it to be made in high yields (>90%) at targeted molecular weights.[24]

View Article Online
DOI: 10.1039/C7TA03103C

To explore the suitability of PCDTBT as a solution-processable HTM in perovskite solar cells, we have fabricated devices employing an efficient multi-cation, multi-halide perovskite active layer based on formamidinium lead iodide ($FAPbI_3$) and methylammonium lead bromide ($MAPbBr_3$), as adapted from previous work.[7] We note that doped-PCDTBT has previously been used as an HTM in standard architecture (n-i-p) PSCs; however, device efficiency was relatively low at 4.2%.[17] Here, we show that by optimising both PCDTBT thickness and doping level, devices based on the structure [FTO/c-TiO_2/mp-TiO_2/$(FAPbI_3)_{0.85}$ $(MAPbBr_3)_{0.15}$/PCDTBT/Au] can be created having a peak efficiency of 15.9% PCE. This efficiency compares very well with our control PSC devices incorporating a spiro-OMeTAD HTM (doped with LiTFSI, TBP and FK209) that have a peak efficiency of 17.4%. To achieve such performance, PCDTBT is combined with the materials most commonly used in high efficiency spiro-OMeTAD-PSCs; namely LiTFSI, FK209 and TBP. Our champion devices also employ a LiTFSI layer above the mesoporous (mp) TiO_2 electron-selective contact. This approach is based on other recent reports, whereby such an LiTFSI layer generated an improvement in device metrics via a reduction in nonradiative recombination at defect sites at the surface of the TiO_2.[25,26] As part of our optimisation studies, we explore the optical, electronic and structural properties of doped and undoped PCDTBT using a range of techniques, including UV-vis absorption spectroscopy, grazing-incidence wide-angle X-ray scattering (GIWAXS), atomic force microscopy (AFM), and thin-film conductivity measurements. Our approach allows us to determine the effect of the dopants on the polymer and the doping level required to optimise device efficiency. We also compare the photo-stability of doped and undoped PCDTBT with that of spiro-OMeTAD and present preliminary findings that suggest that PCDTBT may well allow perovskite solar cells to be fabricated having enhanced operational stability.

View Article Online
DOI: 10.1039/C7TA03103C

2. Results and discussion

We first describe the effects that doping PCDTBT has on its optical and electronic structure. In Figure 1 we present the chemical structures of PCDTBT (a) and spiro-OMeTAD (b) together with the materials added to the HTMs: FK209 (c), TBP (d), and LiTFSI (e). Figure 1(f) shows the UV-Vis absorption of FK209 and a 1:5.6 molar ratio blend of LiTFSI:TBP dissolved into acetonitrile. It can be seen that FK209 is characterised by an absorption band with an onset located at 550 nm, while the LiTFSI:TBP has a weaker absorption peaking at 440 nm with an absorption onset also occurring at 550 nm. In Figure 1(g), we plot the absorption of a thin-film PCDTBT (red) and spiro-OMeTAD (black) when they are doped with LITFSI, TBP and FK209 at a molar ratio (normalised to the molar concentration of PCDTBT monomer) of 1:0.4:2.4 for PCDTBT:LiTFSI:TBP and 1:0.2:0.8:0.03 for spiro-OMeTAD:LiTFSI:TBP:FK209. The absorbance spectra PCDTBT is characterised by broad absorption bands at 390 and 510 nm, corresponding to electronic transitions from the S_0 ground state to S_2 and S_1 (charge-transfer like) excited states.[27] We see very little difference between the absorption spectra of the doped and undoped PCDTBT, and conclude that at the concentration used, the dopants do not appear to modify its absorbance spectra. In Figure S1, we confirm that the molar attenuation of LiTFSI and TBP dopants is insignificant relative to that of PCDTBT.

Figure 1(h) compares to the photo-stability of doped and undoped PCDTBT and spiro-OMeTAD with 1:0.4:2.4:0.052 PCDTBT:LiTFSI:TBP:FK209 and 1:0.2:0.8:0.03 spiro-OMeTAD:LiTFSI:TBP:FK209 respectively. Here, films of equivalent thickness were placed in air under a halogen lamp emitting light having a brightness equivalent to 1 sun. Samples were then periodically removed from under the lamp and their optical absorption re-measured. It can be seen that the peak optical absorption of the undoped PCDTBT reduces to 80% of its initial value after 10 hours. The absorption of the undoped spiro-OMeTAD however reduces

View Article Online
DOI: 10.1039/C7TA03103C

less rapidly, and falls to 80% of its initial value after around 30 hours of illumination. It is clear that compared to spiro-OMeTAD, PCDTBT has a significantly increased absorption across the visible spectrum, and thus the more rapid photo-degradation observed here is consistent with an enhanced rate of excited state generation that increases photo-oxidation.

Upon doping however, both spiro-OMeTAD and PCDTBT films are more photostable, with the absorption of doped PCDTBT and spiro-OMeTAD films estimated to reduce to 80% of their initial value after 75 hours. Interestingly, the doped PCDTBT film has a similar photostability to that of the doped spiro-OMeTAD despite the fact that it absorbs a greater flux of the incident photons. We attribute the increased photostability of the films on doping to exciton quenching by the dopants; a process that appears to reduce the rate of excited-state photochemical reactions that generate non-radiative defects. This is confirmed by steady state photoluminescence measurements (see Figure S2) made on doped and undoped PCDTBT films, that indicate a partial quenching (by 33%) of PCDTBT luminescence.

In the supplementary information (see Figure S3) we compare the contact angle of doped and undoped PCDTBT and spiro-OMeTAD films to deionised water using a sessile drop technique. This demonstrates that in both its doped and undoped forms, PCDTBT is significantly more hydrophobic than spiro-OMeTAD. Indeed, upon addition of the hydrophilic dopants into the films, the contact angle of spiro-OMeTAD drops by over 20°, while the contact angle of PCDTBT undergoes a negligible change (limited to a reduction of 2º). This indicates that spiro-OMeTAD is more likely to absorb water onto its surface than PCDTBT, and may thus present a less effective barrier to the migration of moisture in an operational device.

To further understand the effect of the dopants on the PCDTBT we have performed GIWAXS measurements to determine the effect of the dopants on molecular packing.

View Article Online
DOI: 10.1039/C7TA03103C

Typical data is shown in Figure S4. We find that the doping levels used do not apparently result in significant shifts of either the lamella-separated side chains or the π-π stacked backbones, indicating that the dopant molecules are unlikely to directly intercalate between chains. However we find a degree of broadening of all scattering features that is accompanied by a relative reduction in intensity of the lamella-scattering peak, indicative of a general increase in film disorder.[28,29] We propose therefore that the molecular dopants mix with the PCDTBT at a mesoscopic level which leads to partially disrupted molecular packing.

To prepare doped PCDTBT films for use as an HTM layer, the LiTFSI, TBP, FK209 were added to the solutions at different concentrations, with the solutions then cast into thin-films by spin-coating. However, it was found that when FK209 was added to PCDTBT (in excess of a molar ratio PCDTBT:FK209 of 1:0.052 in a 20mg/ml PCDTBT CB solution), the solid component of the solution underwent aggregation as evidenced by increased solution turbidity. Indeed, this effect can be evidenced through AFM and optical images of doped and undoped spin-cast PCDTBT thin films as shown in Figure 2. For films doped containing LiTFSI and TBP, the AFM image shown in Figure 2(b) and optical image shown in Figure 2(e) indicate the presence of small aggregates that increase film roughness by approximately four times compared to that of undoped PCDTBT (corresponding to a surface roughness of 2.6 nm and 0.61 nm respectively). Upon addition of FK209, at a FK209 doping ratio of 1:0.03 PCDTBT:FK209, doped films of PCDTBT form a continuous film having a roughness of 3.1 nm, as determined using AFM (see Figure 2(c)). However, at longer length-scales (see Figure 2(f)), it is apparent that such films contain aggregates having length-scales as large as 100 μm, making them unsuitable for PV applications.

To understand the effect of chemical doping on the electronic properties of PCDTBT, we have measured its electronic conductivity in both its doped and undoped states. This was done by spin-casting PCDTBT solutions containing the various dopants at different

View Article Online
DOI: 10.1039/C7TA03103C

concentrations onto interdigitated ITO electrodes (supplied by Ossila Ltd), in which the lateral spacing between electrode contacts varied between 50 and 200 μm. Current-voltage scans were then performed, and the effective film conductivity was extracted.

Figure 3(a) plots the conductivity of a PCDTBT film when doped with LiTFSI, TBP or FK209, or with a blend of LiTFSI and TBP, or with LiTFSI, TBP and FK209. It can be seen that PCDTBT films doped with TBP have a conductivity that its less than 1 order of magnitude greater than undoped PCDTBT. We believe however that the conductivity quoted here for the undoped PCDTBT must be seen as an upper-limit of its actual conductivity, as our measurement is limited by the current resolution of the source-measure unit used to perform the measurement. Doping PCDTBT with either LiTFSI or FK209 results in a significant increase in conductivity of between 6 and 7 orders of magnitude. Notably, the additional inclusion of TBP does not result in a significant further increase in conductivity, with the conductivity of the LiTFSI:TBP doped PCDTBT film being around 6×10^{-4} S m^{-1}. Upon further addition of FK209, we find the conductivity of the film with all three dopants increases to 4×10^{-3} S m^{-1}. Such increased conductivity as a result of p-doping is well-known; for example the conductivity of spiro-OMeTAD increases from between 10^{-6} to 10^{-3} S m^{-1} when doped with LiTFSI and/or FK209. [9,30]

To demonstrate that the observed increase in PCDTBT conductivity results from p-doping (rather than being caused by some electro-chemical or ionic current resulting from the field-induced migration of the dopant ions), we have dispersed a similar quantity (grams dopant into grams of polymer) of LiTFSI and TBP into the insulating polymer PMMA. The results of this experiment are shown in Figure 3(b). Here, it can be seen that the conductivity of PMMA increases on addition of dopants from around 2×10^{-9} S m^{-1} to 6×10^{-8} S m^{-1}. Again, the conductivity reported here for the undoped polymer is most likely determined by the sensitivity floor of our source-measure unit used to record the current-voltage trace.

View Article Online
DOI: 10.1039/C7TA03103C

PMMA is a high band-gap insulator material that is characterised by fully saturated bonds along its molecular backbone. Thus, the increase in conductivity seen here most likely originates from the migration of dopants and ions within the film, rather than the formation of a conductive p-doped state. This conductivity level is significantly smaller than that of the doped PCDTBT; a result suggesting that while there may be some small component of ionic movement or electro-chemical current in the doped PCDTBT, it is likely that a different process is responsible for its increased conductivity. We therefore attribute the 10^5 times increase in conductivity in the doped PCDTBT films to electronic conduction via p-doped states. Note we have also explored the apparent p-doping of PCDTBT films stored under various conditions and find a slight increase in PCDTBT conductivity when films have been stored in dry air for 24 hours or exposed to A.M 1.5 radiation for 30 minutes, as shown in Figure S5.

We now discuss the use of a doped-PCDTBT polymer as a HTM in standard structure n-i-p architecture PSC. Here, devices were based on the architecture: glass / TEC 10 FTO / c-TiO_2 / mp-TiO_2 / $(FAPbI_3)_{0.85}(MAPbBr_3)_{0.15}$ / HTM / Au as illustrated in the schematic diagram shown in Figure 4(a). To optimise device efficiency, extensive experiments were conducted to optimise the PCDTBT thickness and doping level. For initial thickness optimisation experiments, the dopant level was fixed at 1:0.4:2.4 (PCDTBT monomer:LiTFSI:TBP), with the total solids concentration in the chlorobenzene solution varying between 5 and 30 mg/ml (see Table S1 for full fabrication details for each PCDTBT layer). As a benchmark, devices are compared with devices incorporating a (470 ± 50) nm thick spiro-OMeTAD HTM doped with LiTFSI:TBP:FK209 (1:0.2:0.8:0.03). Again, the data presented on spiro-OMeTAD based devices was collected after optimisation of thickness and dopant levels.

View Article Online
DOI: 10.1039/C7TA03103C

We display the results of the optimisation experiments for PCDTBT-HTM devices in Figure 5 as a series of box-plots, showing device metrics (PCE, short circuit current (J_{sc}), open circuit voltage (V_{oc}) and fill factor (FF)) as a function of PCDTBT thickness as measured by a Bruker DektakXT profilometer. Figure S6 plots typical J-V sweeps for devices with each thickness of PCDTBT. It can be seen that as the thickness of the PCDTBT is increased from 40 to 170 nm, there is a general increase in all device metrics. Beyond a PCDTBT thickness of 170 nm, the J_{sc} and V_{oc} plateau at around 21 mA/cm^2 and 1V respectively. The FF and PCE attain peak values of 70% and 15.9% respectively at a PCDTBT thickness of (170 ± 20) nm, after which they reduce as thickness increases. Table S1 in supplementary information details the shunt and series resistance for each PCDTBT thickness.

For completeness, we present cross-sectional scanning electron microscope (SEM) images of optimised PSCs based on spiro-OMeTAD and PCDTBT based HTMs in Figure 4(b) and (c) respectively. It can be seen that the SEM images confirm that the optimum PCDTBT thickness is significantly thinner (170 nm) than that used in the spiro-OMeTAD (470 nm) devices. Nevertheless, the PCDTBT films appear to be uniform and successfully form a continuous film over the perovskite active layer. The cross-sectional SEM was performed on champion devices with device metrics in the top quartile of a batch of similar devices. Despite the good performance of these devices, we observe the presence of darker spots in the perovskite layer in both spiro-OMeTAD and PCDTBT devices. An intensity line profile of these spots (see Figure S7) indicates that they are not voids, but contain some material. It is well known that a reduced signal of back-scattered electrons may indicate a specimen with lower average atomic number.[31] However, under the imaging conditions used here, n-type material would also appear darker than undoped or p-doped regions.[32,33] These darker regions could therefore be either residual organic material from fabrication, an onset

View Article Online
DOI: 10.1039/C7TA03103C

of perovskite degradation into its organic components, or dopant-heavy regions of the perovskite. We also note the presence of a darker region of the HTM near the perovskite/HTM interface, which we attribute to a build-up of n-doped material. It is likely this is further evidence for the origin of band bending which is likely beneficial to hole extraction. Further investigation is needed to understand the origin of these darker regions, and their presence indicates that further improvements in device performance, beyond those reported here, may be possible.

We have explored the effects of doping the PCDTBT HTM at various levels on the performance of a PSC device. In all cases, the thickness of the PCDTBT HTM was fixed at 170 nm. Table 1 summarises key metrics of devices constructed using PCDTBT doped with a combination of materials at different concentrations. It can immediately be seen that the undoped PCDTBT HTM results in devices having very low PCEs of (0.37 ± 0.04)% as a result of low J_{sc} and FF. It is likely that the low conductivity and lack of band bending in the undoped PCDTBT film impedes hole transport from the perovskite active layer to the Au contact. It can be seen that devices incorporating PCDTBT doped with LiTFSI or FK209 have improved performance, however, the device PCE is limited to (0.98 ± 0.5)% and (1.94 ± 0.7)% respectively. This indicates that hole extraction from devices without TBP is still highly inefficient despite the large increase in conductivity observed in PCDTBT films doped with either LiTFSI or FK209, as evidenced in Figure 3. Interestingly, devices in which the PCDTBT is doped with TBP perform much better, having a PCE of (6.6 ± 1.5)%, indicating that it is the most critical of the dopants explored. Here, such gains in efficiency result from significantly increased J_{sc}. We note that previous work has suggested that a build-up of TBP at the interface between the perovskite and various HTMs (e.g. spiro-OMeTAD and single-walled carbon nanotubes capped by the polymer PMMA) may induce band bending and enhance the band alignment between the perovskite valance band and the HTM HOMO

View Article Online
DOI: 10.1039/C7TA03103C

level,[15] resulting in more effective hole transfer. Here we assume that a similar effect occurs, with the low values for device FF being consistent with the low conductivity of the TBP-doped PCDTBT without LiTFSI.

When both LiTFSI and TBP are doped into the PCDTBT at a concentration of (1:0.4:2.4) and at an enhanced concentration of (1:0.8:4.8) (referred to as x2 in Table 1), we find a significant enhancement of device metrics. Here, devices utilising the PCDTBT at the 'standard' doping level have a PCE of (14.4 ± 0.7)%; a value that is apparently reduced to (11.8 ± 1.0)% at the x2 concentration. Here, the reduction in efficiency at the enhanced doping level results from a reduction in all device metrics apart from V_{oc}. It has been proposed that LiTFSI passivates trap states at the TiO_2 surface, increasing the V_{oc} but increasing charge recombination rates at the perovskite/TiO_2 interface,[10,34] which may explain the reduction in x2 doped device performance. We also find that as the concentration of dopants is increased, the doped PCDTBT solution becomes increasingly harder to wet to the perovskite surface.

Upon addition of all dopants (LiTFSI, TBP and FK209) to the PCDTBT, we find a reduction in all device metrics, with the PCE reducing to (12.7 ± 1.2)%. It appears that despite the fact that such films have the highest conductivity (see Figure 3), the enhanced film inhomogeneity (see Figure 2) acts to reduce device efficiency. We believe this is consistent with an increase in the number short circuit pathways between the perovskite and metal contact.

It appears, therefore, that PCDTBT achieves best performance as a HTM when it is used at a thickness of around (170 ± 20) nm and doped with LiTFSI and TBP at a molar ratio of 1:0.4:2.4 for PCDTBT monomer:LiTFSI:TBP. We compare the performance of batches of these device with a batch of devices incorporating a spiro-OMeTAD HTM, in addition to champion metrics for devices that incorporate an additional LiTFSI interlayer above the mp-

View Article Online
DOI: 10.1039/C7TA03103C

TiO_2 in Table 2. As has been previously reported, there is an increase in FF upon the inclusion of the Li-TFSI interlayer,[26] but no significant change in other device metrics. For completeness, we plot JV curves under AM1.5 illumination for PSCs based on a PCDTBT and spiro-OMeTAD HTMs, containing a LiTFSI interlayer, in Figure 6(a), and include stabilised measurements of output power in Figure 6(b). It can be seen that devices incorporating the PCDTBT HTM have a slightly reduced performance compared to those using the spiro-OMeTAD HTM (peak PCE of 15.9% compared with 17.4%). This reduction in efficiency mainly occurs as a result of lower FF (70% compared to 73% for PCDTBT and spiro-OMeTAD HTMs respectively).

Finally, we have made preliminary measurements of operational stability on devices utilising doped PCDTBT (see Figure S8) that are compared to benchmark devices utilising a doped spiro-OMeTAD HTM. Here, devices were deliberately left unencapsulated, and operated in air under a constant 1 sun equivalent halogen lamp. It was found that after 75 hours, the PCE of PCDTBT had reduced to 50% of its initial value. In comparison, devices utilising a spiro-OMeTAD HTL had reduced to 30% of their initial efficiency over the same period. We suspect that the enhanced stability of devices incorporating a PCDTBT HTM may result from its hydrophobic nature (even upon doping) that reduces the ingress of moisture into the perovskite active layer.

3. Conclusions

We have explored doping the conjugated polymer PCDTBT with a series of dopant molecules to improve its functionality as a hole-transport material in a perovskite solar cell. Electrical measurements indicate that the conductivity of PCDTBT thin films was increased by a factor of ~10^5 times upon doping with LiTFSI and TBP, making it ideal a material for efficient charge transport. Comparative light-soaking measurements suggest that the

View Article Online
DOI: 10.1039/C7TA03103C

photostability of doped PCDTBT is comparable to that of doped spiro-OMeTAD, while contact angle measurements suggest that doped PCDTBT has a more hydrophobic surface, suggesting an enhanced barrier to the ingress of moisture. X-ray scattering measurements on doped and undoped thin films of PCDTBT indicated that both the lamelle and π–π stacking peaks were broadened in the doped films suggesting that the chemical doping may partially disrupt molecular packing. The LiTFSI and TBP doped PCDTBT films were then used as a HTM in standard architecture PSCs. Here, it was found that using either LiFISI and TBP alone did not markedly improve device performance, however it was the combined use of such dopants that was necessary to improve device efficiency. By optimising the doping level and thickness of the doped PCDTBT HTM layer, PSC devices were created with a champion PCE of 15.9%, with stabilised measurements performed under ambient conditions revealing device efficiencies of 13.2%. Our work confirms that doped PCDTBT is a promising HTM in high-performance perovskite solar cell devices.

Experimental Methods

Device fabrication: All solvents used were purchased from Sigma Aldrich. Devices were fabricated on TEC 10 FTO/glass substrates (XOP glass). FTO was patterned by etching each substrate with zinc powder and 4M HCl, after which they were dumped in DI water, dried and swabbed with cotton buds and then sonicated for 10 minutes in hot Helmanex detergent solution, twice in deionised water, and IPA. The c-TiO_2 layer was deposited by spray-pyrolysis from a dilution of 1.72ml of Titanium diisopropoxide bis(acetylacetonate) (75wt % Sigma Aldrich) in 18.28ml of IPA (Sigma Alrich) onto a hotplate at 450^{o}C and left to sinter for 30 minutes.

A meso-porous TiO_2 (mp-TiO_2) layer was fabricated from a titanium oxide paste (18-NRT Dyesol) that was first diluted to 15 wt% in ethanol. The resulting solution was spin coated in air (< 35% RH) at room temperature on top of the c-TiO_2 at 5000 rpm for 15s. After

View Article Online
DOI: 10.1039/C7TA03103C

deposition, the substrates were left at room temperature for 10 minutes before being sintered in air for 1 hour at 450°C. For final champion devices a 19mg/ml solution of bis(trifluoromethane)sulfonimide lithium salt, LiTFSI (Sigma Aldrich) in acetonitrile was spun onto the substrates in air (<35% RH) at 3000rpm and the substrates were re-sintered in air at 450°C for a further 30 minutes before being passed into a nitrogen filled glove box.

To prepare the perovskite layer, formamidinium iodide FAI (>99.5%, Ossila), lead iodide PbI_2 (99%, Sigma Aldrich), methylammonium bromide MABr (Dyesol) and lead bromide $PbBr_2$ (99.999%, Sigma Aldrich) were dissolved in a 4:1 v/v DMF:DMSO solvent blend at a concentration of 1.31M, 1.38M, 0.24M, 0.24M for FAI, PbI_2, MABr and $PbBr_2$ respectively. This produced a ~50% wt $(FAPbI_3)_{0.85}(MAPbBr_3)_{0.15}$ perovskite solution, however the 0.95:1 FAI:PbI_2 molar ratio used resulted in a slight excess of lead in the final solution. The resultant ink was not heated and has not yet been shown to be stable beyond 1 week when stored in air.

To process the perovskite precursor, the $(FAPbI_3)_{0.85}(MAPbBr_3)_{0.15}$ solution was deposited inside an N_2 filled glovebox using a 2-step anti-solvent spin routine adapted from Bi, D. et al.[7] Firstly 50µl of the perovskite solution was dispensed onto the stationary substrate from a pipette. The substrate was then spun at 2000 rpm for 10 s with a ramp-up of 200 $rpms^{-1}$ then at 6000 rpm for 30 s with a ramp-up of 2000 $rpms^{-1}$. A near continuous stream of 100µl of chlorobenzene was then rapidly deposited onto the spinning substrate after 10 seconds into the second stage of the spin cycle (corresponding to 20 seconds after the perovskite was originally dispensed). Immediately after spin-casting, the substrate was placed on a hotplate at 100°C and annealed for 90 minutes.

To prepare the PCDTBT layer, A low palladium content poly[N-9'-heptadecanyl-2,7-carbazole-alt-5,5-(4',7'-di-2-thienyl-2',1',3'-benzothiadiazole)], PCDTBT with Mw ~ 34,900 (Ossila) (synthesised as described in ref [19] and purified as described in ref [21]) was first

View Article Online
DOI: 10.1039/C7TA03103C

dissolved in chlorobenzene (CB) at 20mg/ml. Similarly, spiro-OMeTAD (2,2',7,7'-Tetrakis[N,N-di(4-methoxyphenyl)amino]-9,9'-spirobifluorene) (> 99.5% Ossila) was first dissolved in CB at 96.6mg/ml. Stock dopant solutions of LiTFSI (Sigma) and FK 209 Co(III) - TFSI (Dyesol) were made at 175mg/ml in acetonitrile. To achieve the standard (optimum) doping level, 20µl of LiTFSI stock and 10µl of TBP (96%, Sigma) were added to 1ml of PCDTBT solution. The optimum spiro-OMeTAD solutions were created by adding 30µl of LiTFSI stock, 10µl of TBP and 20µl of FK209 stock to 1ml of spiro-OMeTAD solution. This was equivalent to a molar ratio of 1:0.4:2.4 for PCDTBT monomer:LiTFSI:TBP and 1:0.2:0.8:0.03 for spiro-OMeTAD:LiTFSI:TBP:FK209. For PCDTBT thickness screening the dopant ratio was held constant and solution concentrations were scaled as indicated in Table S1. For PCDTBT HTMs using FK209, 3.2µl of stock FK209 was added to 250 µl of doped PCDTBT solution. All solutions were kept at room temperature and vortex mixed before use. For optimum device performance, HTMs were spun at 2000rpm for 30s onto a static perovskite coated substrate in a nitrogen filled glovebox. For thickness tuning measurements the spin speed was changed as indicated in Table S1. Thicknesses were measured using a Bruker DektakXT profilometer.

To deposit the device anode, the devices were returned into air and placed in an Edwards Auto 306 bell-jar evaporator. An 80nm thick gold layer was evaporated onto the device surface at a pressure of *ca* 10^{-6} mbar. The final device layout is shown in Figure S9.

Absorption: UV-vis measurements were performed under ambient conditions using UV-VIS-NIR light source (Ocean Optics – DH-2000-BAL), collection fibre optic cables (Ocean Optics) and spectrometer (Ocean Optics – HR2000+ES). Samples for absorption measurements were prepared on quartz-coated glass using the same deposition methods as used in device fabrication. Doped samples were made with doping levels that match those

View Article Online
DOI: 10.1039/C7TA03103C

described in device fabrication. Doped and undoped HTM films of 120-140nm, matching the doping level used in champion devices, were aged under a constant 1 sun equivalent halogen lamp containing a UV component.

Solution absorption measurements of the dopants were recorded in a clean cuvette having a 0.4 cm path length, using doping levels equivalent to 1/3 the dopant level used to make champion PCDTBT devices. Supplementary solutions were taken with diluted 0.0125mg/ml PCDTBT solution in CB with doping concentrations of x320 LiTFSI, TBP and x240 FK209 relative to device doping levels.

Contact Angle: A goniometer tensiometer coupled with Attension Theta software package was used to take images of static droplets of deionized water on doped and undoped PCDTBT and spiro-OMeTAD films and determine the sessile contact angle.

GIWAX S: Grazing Incidence Wide-Angle X-ray Scattering (GIWAXS) measurements were carried out using a Xenocs Xeuss 2.0 SAXS/WAXS machine equipped with was a liquid Gallium MetalJet (Excillum) x-ray source emitting x-rays with an energy of 9.2 keV. PCDTBT samples with (~120 nm thick) and without the dopants (~90 nm thick) were mounted on an angular positioning stage to align the samples. The measurements were performed in a vacuum chamber to reduce the background signal. The scattered X-rays were measured with a Pilatus3R 1M detector over a count time of 10 minutes. The 2D detector image was processed using Foxtrot software, which was used to produce the 1D plots.

Atomic Force Microscopy: A Veeco Dimension 3100 operated in tapping mode with was used to characterise undoped, LiTFSI and TBP doped and FK209 doped PCDTBT films equivalent to those used in device fabrication.

View Article Online
DOI: 10.1039/C7TA03103C

Conductivity: Samples for conductivity measurements were prepared on Interdigitated (ID) ITO Substrates with variable channel width, 50 to 200 μm (Ossila). Undoped and doped ITO/PCDTBT/ITO samples were made with doping levels that also match those described in device fabrication. The conductivity was extracted from the high E-field region, beyond the charge injection inflections of I-V scans measurements, taken using a Keithley 237 source measure unit to sweep from -10 V to +10V and back again at various scan speeds on samples with various channel widths. For the poly(methyl methacrylate) PMMA measurements a 5mg/ml solution of Mw ~ 120,000 (Sigma) in CB was dispensed with and without 5μl of LiTFSI stock and 2.5μl of TBP. Since the density of a film of PMMA and PCDTBT are similar (both ~ 1.2 $g.cm^{-3}$)[35,36], the same ratio of doping concentrations was used for both materials and are assumed comparable.

SEM: An FEI Nova Nano 450 scanning electron microscope (SEM) was used to image PSC devices. Here, fractured samples were attached to 1 cm diameter stubs using electrically conductive silver paint and allowed to dry before being loaded into the SEM. All the samples were imaged using through-lens detector (TLD) with a beam current of ~21 pA and an accelerating voltage of 1.5 kV.

Device characterisation: Device performance was determined by measuring J-V curves under ambient conditions using a Newport 92251A-1000 solar simulator. A NREL certified silicon reference cell was used to calibrate the simulated AM1.5 light to 100 $mWcm^{-2}$ at 25°C. The un-encapsulated devices were covered with an illumination aperture mask that defined an illuminated area of 0.0256 cm^2. J-V measurements were recorded using a Keithley 237 source measure unit that swept the applied bias from -1.2 V to +1.2V and back again at a scan

View Article Online
DOI: 10.1039/C7TA03103C

speed of 0.4 Vs^{-1}. The J-V scans were typically recorded on the second or third day after device fabrication. The performance metrics were extracted from the J-V scan and then used to determine the V_{mpp} of the best devices. Stabilised current/power measurements were taken by holding the devices at their V_{mpp} for several minutes. For supplementary device stability data, several PSCs of starting PCEs equivalent to those reported here, implementing PCDTBT (doped with FK209 in addition to LiTFSI and TBP) and spiro-OMeTAD as HTMs, are repeatedly tested in air at 45^{o}C with uncontrolled humidity, under a constant AM 1.5 light source. Devices are left without encapsulation to accelerate the degradation process. The device metrics are normalised to several reference diodes.

Supporting Information

Supporting Information is available online.

Acknowledgements

This work was funded by the UK Engineering and Physical Sciences Research Council (EPSRC) via grants EP/M025020/1 'High resolution mapping of performance and degradation mechanisms in printable photovoltaic devices', EPSRC grant EP/N008065/1 'SECONDARY ELECTRON EMISSION - MICROSCOPY FOR ORGANICS WITH RELIABLE ENGINEERING-PROPERTIES', and EP/M014797/1 'Improved Understanding, Development and Optimization of Perovskite-based Solar Cells'. We also thank the EPSRC for PhD studentships via the University of Sheffield DTG account (J.B.) and from the Centre for Doctoral Training in New and Sustainable PV, EP/L01551X/1 (M.S.). We also would like to thank Dr Andrew J Musser and Dr David Coles for useful discussions. The GIWAXS

View Article Online
DOI: 10.1039/C7TA03103C

measurements were made possible by the recently installed Xeuss 2.0 instrument, and we are grateful to Xenocs for their help and support in the user program at Sheffield.

Received: ((will be filled in by the editorial staff))
Revised: ((will be filled in by the editorial staff))
Published online: ((will be filled in by the editorial sta

References

[1] M. Saliba, T. Matsui, K. Domanski, J.-Y. Seo, A. Ummadisingu, S. M. Zakeeruddin, J.-P. Correa-Baena, W. R. Tress, A. Abate, A. Hagfeldt, M. Gratzel, *Science (80).* **2016**, *5557*.

[2] G. Grancini, C. Rolda´n-Carmona, I. Zimmermann, E. Mosconi, X. Lee, D. Martineau, S. Narbey, F. Oswald, F. De Angelis, M. Graetzel. M. K. Nazeeruddin, *Nat. Commun.* **2017**, *8,* 15684.

[3] S. Ameen, M. A. Rub, S. A. Kosa, K. A. Alamry, M. S. Akhtar, H. S. Shin, H. K. Seo, A. M. Asiri, M. K. Nazeeruddin, *ChemSusChem* **2016**, *9*, 10.

[4] S. F. Völker, S. Collavini, J. L. Delgado, *ChemSusChem* **2015**, *8*, 3012.

[5] M. M. Lee, J. Teuscher, T. Miyasaka, T. N. Murakami, H. J. Snaith, *Science* **2012**, *338*, 643.

[6] M. Saliba, T. Matsui, J.-Y. Seo, K. Domanski, J.-P. Correa-Baena, N. Mohammad K., S. M. Zakeeruddin, W. Tress, A. Abate, A. Hagfeldt, M. Gratzel, *Energy Environ. Sci.* **2016**, *9*.

[7] D. Bi, W. Tress, M. I. Dar, P. Gao, J. Luo, C. Renevier, K. Schenk, A. Abate, F.

View Article Online
DOI: 10.1039/C7TA03103C

Giordano, J.-P. Correa Baena, J.-D. Decoppet, S. M. Zakeeruddin, M. K. Nazeeruddin, M. Gra tzel, A. Hagfeldt, *Sci. Adv.* **2016**, *2*, e1501170.

[8] T. Leijtens, G. E. Eperon, S. Pathak, A. Abate, M. M. Lee, H. J. Snaith, *Nat. Commun.* **2013**, *4*, 2885.

[9] J. H. Noh, N. J. Jeon, Y. C. Choi, M. K. Nazeeruddin, M. Grätzel, S. Il Seok, *J. Mater. Chem. A* **2013**, *1*, 11842.

[10] S. Wang, W. Yuan, Y. S. Meng, *ACS Appl. Mater. Interfaces* **2015**, *7*, 24791.

[11] Y. Liu, Q. Chen, H.-S. Duan, H. Zhou, Y. Yang, H. Chen, S. Luo, T.-B. Song, L. Dou, Z. Hong, Y. Yang, *J. Mater. Chem. A* **2015**, *3*, 11940.

[12] W. H. Nguyen, C. D. Bailie, E. L. Unger, M. D. Mcgehee, *JACS* **2014**, *136*, 10996.

[13] G. Schlichthörl, S. Y. Huang, J. Sprague, a J. Frank, *J. Phys. Chem. B* **1997**, *101*, 8141.

[14] S. Wang, M. Sina, P. Parikh, T. Uekert, B. Shahbazian, A. Devaraj, Y. S. Meng, *Nano Lett.* **2016**, acs. nanolett.6b02158.

[15] S. N. Habisreutinger, N. K. Noel, H. J. Snaith, R. J. Nicholas, *Adv. Energy Mater.* **2016**, 1601079.

[16] Y.-K. Wang, Z.-C. Yuan, G.-Z. Shi, Y.-X. Li, Q. Li, F. Hui, B.-Q. Sun, Z.-Q. Jiang, L.-S. Liao, *Adv. Funct. Mater.* **2016**, *26*, 1375.

[17] J. H. Heo, S. H. Im, J. H. Noh, T. N. Mandal, C.-S. Lim, J. A. Chang, Y. H. Lee, H. Kim, A. Sarkar, K. NazeeruddinMd, M. Gratzel, S. Il Seok, *Nat Phot.* **2013**, *7*, 486.

[18] Y. Zhang, E. Bovill, J. Kingsley, A. R. Buckley, H. Yi, A. Iraqi, T. Wang, D. G.

View Article Online
DOI: 10.1039/C7TA03103C

Lidzey, *Sci. Rep.* **2016**, *6*, 21632.

[19] N. Blouin, A. Michaud, M. Leclerc, *Adv. Mater.* **2007**, *19*, 2295.

[20] S. Beaupré, M. Leclerc, *J. Mater. Chem. A* **2013**, *1*, 11097.

[21] C. Bracher, H. Yi, N. W. Scarratt, R. Masters, A. J. Pearson, C. Rodenburg, A. Iraqi, D. G. Lidzey, *Org. Electron.* **2015**, *27*, 266.

[22] E. S. R. Bovill, J. Griffin, T. Wang, J. W. Kingsley, H. Yi, A. Iraqi, A. R. Buckley, D. G. Lidzey, *Appl. Phys. Lett.* **2013**, *102*.

[23] S. S. Reddy, K. Gunasekar, J. H. Heo, S. H. Im, C. S. Kim, D. H. Kim, J. H. Moon, J. Y. Lee, M. Song, S. H. Jin, *Adv. Mater.* **2016**, *28*, 686.

[24] S. Wakim, S. Beaupré, N. Blouin, B.-R. Aich, S. Rodman, R. Gaudiana, Y. Tao, M. Leclerc, *J. Mater. Chem.* **2009**, *19*, 5351.

[25] M. Saliba, T. Matsui, J.-Y. Seo, K. Domanski, J.-P. Correa-Baena, M. K. Nazeeruddin, S. M. Zakeeruddin, W. Tress, A. Abate, A. Hagfeldt, M. Grä Tzel, **2016**, *9*, 1989.

[26] F. Giordano, A. Abate, J. Pablo, C. Baena, M. Saliba, T. Matsui, S. H. Im, S. M. Zakeeruddin, M. K. Nazeeruddin, A. Hagfeldt, M. Graetzel, *Nat. Commun.* **2016**, *7*, 1.

[27] N. Banerji, E. Gagnon, P. Y. Morgantini, S. Valouch, A. R. Mohebbi, J. H. Seo, M. Leclerc, A. J. Heeger, *J. Phys. Chem. C* **2012**, *116*, 11456.

[28] T. Wang, A. J. Pearson, A. D. F. Dunbar, P. A. Staniec, D. C. Watters, D. Coles, H. Yi, A. Iraqi, D. G. Lidzey, R. A. L. Jones, *Eur. Phys. J. E* **2012**, *35*, 2.

[29] T. Wang, A. J. Pearson, A. D. F. Dunbar, P. A. Staniec, D. C. Watters, H. Yi, A. J. Ryan, R. A. L. Jones, A. Iraqi, D. G. Lidzey, *Adv. Funct. Mater.* **2012**, *22*, 1399.

View Article Online
DOI: 10.1039/C7TA03103C

[30] A. Abate, T. Leijtens, S. Pathak, J. Teuscher, R. Avolio, M. E. Errico, J. Kirkpatrik, J. M. Ball, P. Docampo, I. McPherson, H. J. Snaith, *Phys. Chem. Chem. Phys.* **2013**, *15*, 2572.

[31] J. Cazaux, *J. Microsc.* **2004**, *214*, 341.

[32] C. Schönjahn, R. F. Broom, C. J. Humphreys, A. Howie, S. A. M. Mentink, *Appl. Phys. Lett.* **2003**, *83*, 293.

[33] C. Schönjahn, C. J. Humphreys, M. Glick, *J. Appl. Phys.* **2002**, *92*, 7667.

[34] Q. J. Yu, Y. H. Wang, Z. H. Yi, N. N. Zu, J. Zhang, M. Zhang, P. Wang, *ACS Nano* **2010**, *4*, 6032.

[35] J. Ackermann, M. Juda, D. Hirsch, *Kunststoffe Int.* **2014**, *2014*, 59.

[36] A. J. Clulow, A. Armin, K. H. Lee, A. K. Pandey, C. Tao, M. Velusamy, M. James, A. Nelson, P. L. Burn, I. R. Gentle, P. Meredith, *Langmuir* **2014**, *30*, 1410.

View Article Online
DOI: 10.1039/C7TA03103C

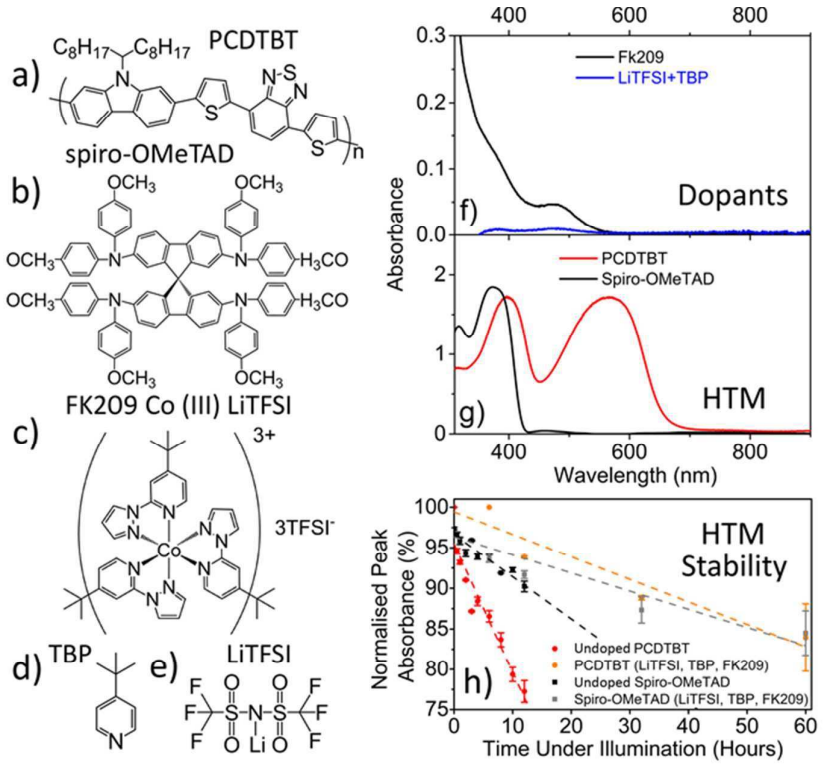

Figure 1: Chemical structures of (a) PCDTBT, (b) spiro-OMeTAD, (c) FK209 Co (III) LiTFSI, (d) TBP and (e) LiTFSI, and absorbance of (f) a solution of 0.78mM FK209 (black) and 4.1mM LiTFSI+ 22.8mM TBP (blue) in acetonitrile, (g) absorbance of doped PCDTBT

View Article Online
DOI: 10.1039/C7TA03103C

(black) and doped spiro-OMeTAD (red). Part (h) shows the decay of the peak absorbance in films of undoped and doped PCDTBT and spiro-OMeTAD films when stored in air under constant AM 1.5 illumination. Details of the doping levels and film thickness are given in the experimental section.

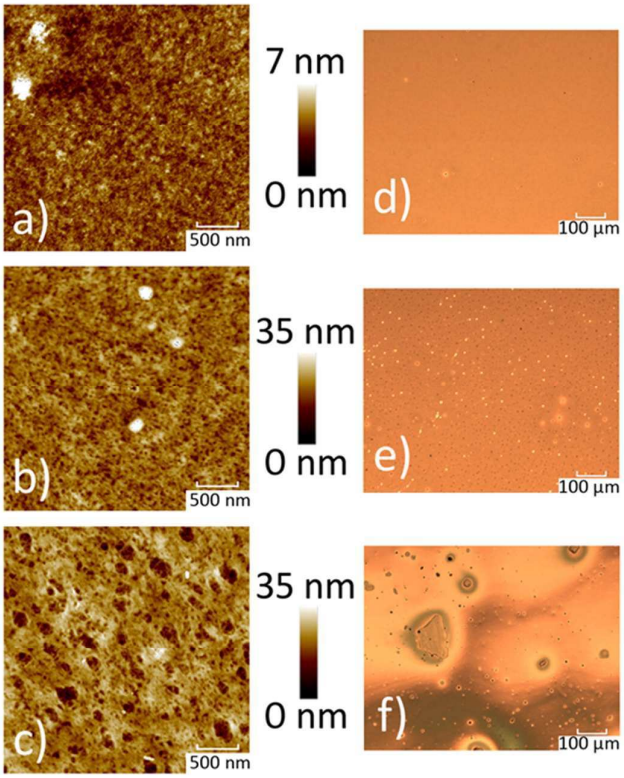

View Article Online
DOI: 10.1039/C7TA03103C

Figure 2: AFM topographs of (a) pure PCDTBT, (b) PCDTBT when doped with LiTFSI + TBP doped, and (c) a PCDTBT film doped with LiTFSI + TBP + FK209. (d), (e) and (f) are optical microscope images of the same films respectively. The film Ra roughness averages are 0.61 nm, 2.6 nm and 3.1 nm respectively.

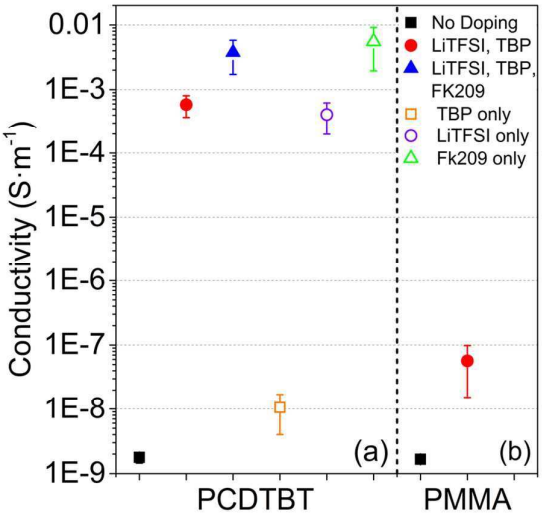

Figure 3: The conductivities of a series of PCDTBT thin films as determined from the high voltage region of I-V traces of films coated on interdigitated ITO substrates. Part (a) shows

View Article Online
DOI: 10.1039/C7TA03103C

the conductivity of a pure PCDTBT film (black), and PCDTBT when doped with LiTFSI + TBP (red), LiTFSI + TBP + FK209 (blue), TBP (orange), LiTFSI (purple) and FK209 (green). Part (b) plots the conductivity of a pure PMMA film (black), and PMMA when doped with LiTFSI + TBP (red).

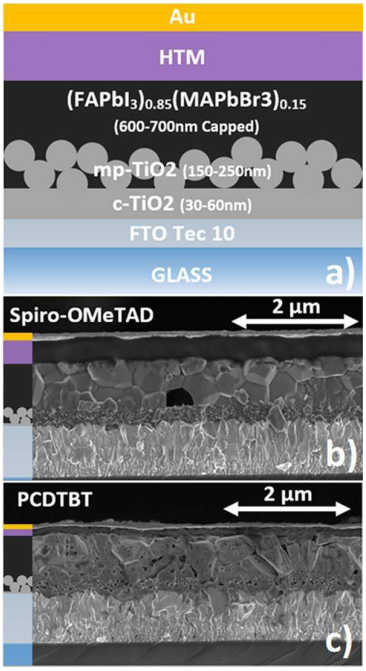

View Article Online
DOI: 10.1039/C7TA03103C

Figure 4: PSC device layout. Part (a) is a schematic figure showing device structure. Part (b) is a cross-sectional scanning electron microscope (SEM) of a reference device using a spiro-OMeTAD HTM (purple). Part (c) shows an SEM image of a device utilising an optimised PCDTBT HTM (purple).

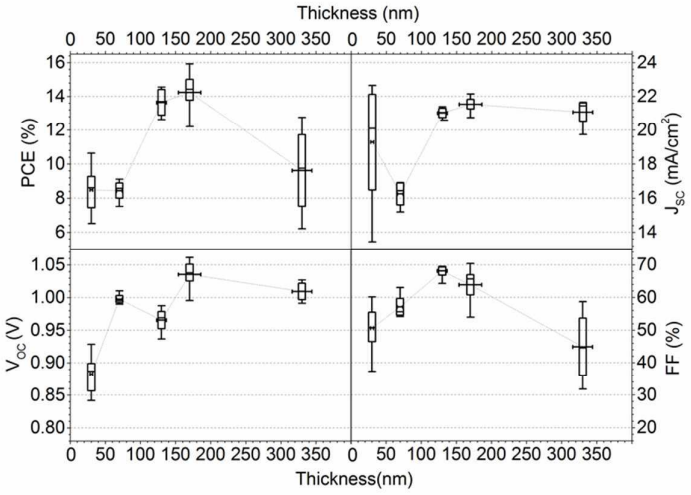

Figure 5: Boxplots of device metrics for a PSC as a function of doped PCDTBT film thickness.

View Article Online
DOI: 10.1039/C7TA03103C

	No Dope	LiTFSI	TBP	LiTFSI,TBP	x2 LiTFSI, x2 TBP	Fk209	Fk209, LiTFSI, TBP
PCE [%]	**0.42** (0.37 ± 0.04)	**2.04** (0.98 ± 0.52)	**8.56** (6.63 ± 1.46)	**15.7** (14.4 ± 0.7)	**12.8** (11.8 ± 1.0)	**3.30** (1.94 ± 0.71)	**15.2** (12.7 ± 1.2)
J_{SC}[mA/cm^2]	**3.8** (3.6 ± 0.3)	**7.9** (5.8 ± 1.3)	**21.2** (20.2 ± 0.8)	**21.6** (20.7 ± 0.7)	**18.5** (17.6 ± 0.9)	**8.3** (5.7 ± 1.6)	**22.4** (21.2 ± 0.9)
V_{oc} [V]	**0.72** (0.69 ± 0.03)	**0.93** (0.83 ± 0.07)	**1.04** (1.01 ± 0.02)	**1.02** (1.01 ± 0.01)	**1.02** (1.00 ± 0.01)	**1.00** (0.90 ± 0.13)	**1.05** (1.02 ± 0.01)
FF [%]	**18** (15 ± 2)	**28** (19 ± 5)	**39** (32 ± 5)	**71** (69 ± 2)	**68** (66 ± 2)	**39** (32 ± 5)	**65** (59 ± 4)

Table 1: Key device metrics for a series of PSCs using a PCDTBT HTM. Data shown in bold text are the peak values obtained with data in parenthesis being the average value ± standard deviation. For the optimum thickness of PCDTBT (170 nm) different PCDTBT data is given for films that are either un-dopded, or doped with LiTFSI only, TBP only, LiTFSI + TBP, double the regular concentration of LiTFSI and TBP, FK209 only, and finally all dopants.

	Spiro-OMeTAD	PCDTBT	Spiro-OMeTAD + LiTFSI Interlayer	PCDTBT + LiTFSI Interlayer
PCE [%]	**16.6** (15.3 ± 0.8)	**15.6** (14.3 ± 0.8)	**17.36**	**15.92**
J_{SC} [mA/cm]	**22.4** (22.0 ± 0.2)	**21.7** (20.7 ± 0.2)	**22.43**	**22.04**
V_{oc} [V]	**1.08** (1.04 ± 0.03)	**1.06** (1.04 ± 0.01)	**1.05**	**1.03**
FF [%]	**70** (67 ± 2.3)	**68** (63 ± 4)	**73**	**70**

View Article Online
DOI: 10.1039/C7TA03103C

Table 2: Key device metrics of optimized PCDTBT-PSCs and reference spiro-OMeTAD-PSCs. Data shown in bold text is peak value obtained with data in parenthesis being the average value ± standard deviation. Key device metrics of our champion devices are also presented, here the devices implement a LiTFSI interlayer above the mp-TiO_2.

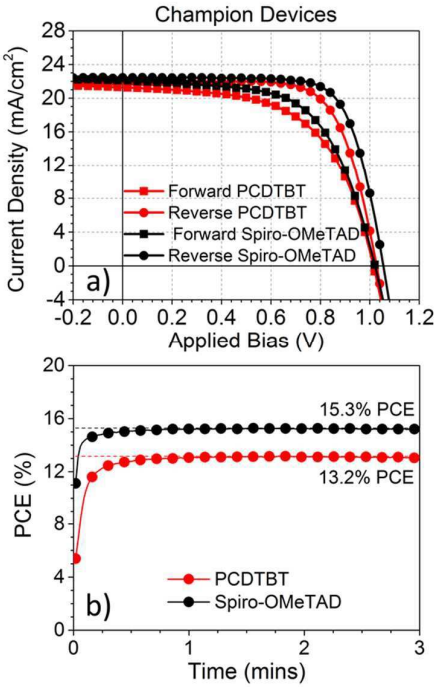

View Article Online
DOI: 10.1039/C7TA03103C

Figure 6: Champion Devices. Part (a) shows J-V curves obtained for champion devices utilising a spiro-OMeTAD HTM (black) and a PCDTBT HTM (red). Forward sweeps indicated by square points and reverse sweeps indicated by circular points. J-V curves were measured at a sweep speed 0.4 Vs^{-1}. (b) Stabilised PCE measurements taken for 3 minutes under constant simulated AM1.5 illumination for spiro-OMeTAD-PSCs (black) and PCDTBT-PSCs (red). These devices implement a Li-TFSI interlayer above the mp-TiO2.

View Article Online
DOI: 10.1039/C7TA03103C

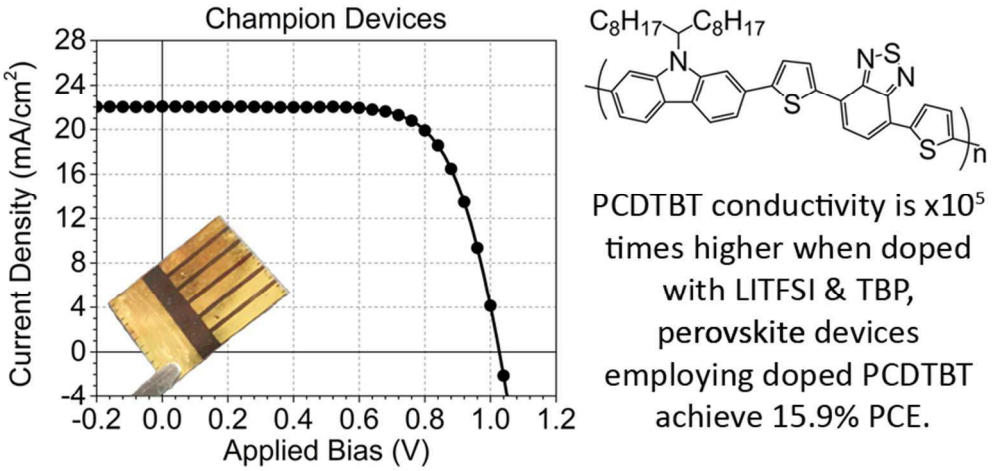

80x40mm (299 x 299 DPI)